


## Protocol Dependence and State Variables in the Force-Moment Ensemble

Ephraim S. Bililign, Jonathan E. Kollmer, and Karen E. Daniels

*Department of Physics, North Carolina State University, Raleigh, North Carolina 27695, USA*

 (Received 26 February 2018; revised manuscript received 11 October 2018; published 23 January 2019)

Stress-based ensembles incorporating temperaturelike variables have been proposed as a route to an equation of state for granular materials. To test the efficacy of this approach, we perform experiments on a two-dimensional photoelastic granular system under three loading conditions: uniaxial compression, biaxial compression, and simple shear. From the interparticle forces, we find that the distributions of the normal component of the coarse-grained force-moment tensor are exponential tailed, while the deviatoric component is Gaussian distributed. This implies that the correct stress-based statistical mechanics conserves both the force-moment tensor and the Maxwell-Cremona force-tiling area. As such, two variables of state arise: the tensorial angoricity ( $\hat{\alpha}$ ) and a new temperaturelike quantity associated with the force-tile area which we name *keramicity* ( $\kappa$ ). Each quantity is observed to be inversely proportional to the global confining pressure; however, only  $\kappa$  exhibits the protocol independence expected of a state variable, while  $\hat{\alpha}$  behaves as a variable of process.

DOI: 10.1103/PhysRevLett.122.038001

Granular systems are characterized by the absence of thermal fluctuations and their ability to maintain a mechanically stable, jammed state in the absence of an external driving force. The formulation of a statistical description of jammed configurational states has been an open question for the behavior of such athermal, macroscopic particles undergoing solely repulsive contact interactions [1–5]. A promising statistical mechanics candidate, the force-moment ensemble, postulates a temperaturelike state variable, conjugate to stress, called angoricity [6]. For simulations of frictionless particles, angoricity has been shown to underpin an equation of state in the microcanonical ensemble [7], and for frictional particles, it has also satisfied a zeroth-law test [8]. However, the correct functional form of the ensemble remains the subject of recent debate [9–14], and the issue is closely tied to recent developments of a general theory of amorphous solids [15,16].

It is also unknown whether such statistical descriptions are appropriate, given that interparticle force distributions and probability densities in configuration space are known to be dependent on the loading protocol [17,18]. Numerous systems, granular [19–21] and otherwise [22,23], encode system history. Furthermore, shear jamming [24,25] is distinct from compressive jamming [26], with the jamming transition occurring over a range of packing fractions and with additional states of minimum shear stress. While some properties of angoricity have been observed in shear-jammed systems [27], there has been no systematic comparison across loading conditions.

To address these questions, we report measurements of particle positions and force-moment tensors for clusters of particles within experiments on a photoelastic granular material; this allows us to measure vector contact forces at

the particle scale. We subsequently extract the granular variables of interest in the force-moment ensemble by making measurements of angoricity for separate tensorial components and loading protocols. We find that this statistical mechanics framework conserves, under configurational perturbations, both the force-moment tensor [28] and the Maxwell-Cremona force-tiling area [11], leading to two protocol-dependent and one protocol-independent conjugate variables.

*Force-moment ensemble.*—By analogy to the equilibrium thermodynamic energy, we calculate the global force-moment tensor [6]  $\hat{\Sigma} = \sum_N \vec{r}_{\mu\nu} \otimes \vec{F}_{\mu\nu}$  over an experiment containing  $N$  particles (enumerated  $\mu, \nu$ ) with centers separated by a displacement  $\vec{r}_{\mu\nu}$  and interparticle contact force  $\vec{F}_{\mu\nu}$ . States of  $\hat{\Sigma}$  are enumerated by the number of configurations  $\Omega(\hat{\Sigma})$  and associated configurational entropy  $S = \ln \Omega$ . The tensorial angoricity is correspondingly defined to be  $\alpha_{ij} = \partial S / \partial \Sigma_{ij}$ , and we expect a Boltzmann-like probability of observing a local cluster of  $m$  nearby particles with local force-moment tensor  $\hat{\sigma}$  within a jammed particulate bath at angoricity  $\hat{\alpha}$ , given by  $\mathcal{P}(\hat{\sigma}|\hat{\alpha}) = \Omega(\hat{\sigma}) e^{-\hat{\alpha}:\hat{\sigma}} / Z(\hat{\alpha})$ , where  $:$  denotes the double inner (scalar) product,  $\hat{\alpha}:\hat{\sigma} = \text{Tr}(\hat{\alpha}^T \hat{\sigma})$ .

As an extension to this theory, we incorporate the effect of the Maxwell-Cremona diagram, which is formed by mapping contact forces to a tiling of contacting polygons, as a representation of static force balance [11]. The total area of the tiling,  $a$ , is a conserved quantity, as rearrangements in force correspond to transfers of area between polygons [10,14]. (Note that, although only frictionless packings sustain strictly convex force tiles, we observe 85% of our tiles to be convex even though they are frictional.) To incorporate this additional conservation

law, we consider an extended Boltzmann-like term to account for the probability of observing a cluster of local force-moment  $\hat{\sigma}$  and tiling area  $a$ :

$$\mathcal{P}(\hat{\sigma}, a|\hat{\alpha}, \kappa) = \frac{\Omega(\hat{\sigma}, a)}{Z(\hat{\alpha}, \kappa)} \exp(-\hat{\alpha}:\hat{\sigma} - \kappa a), \quad (1)$$

where  $\hat{\alpha}$  is the global angoricity associated with  $\hat{\Sigma}$  and  $Z(\hat{\alpha}, \kappa)$  is the partition function [10,13]. We further define  $\kappa = \partial S/\partial a$  as the Lagrange multiplier associated with  $a$ , herein referred to as keramicity (from the Greek word *κεραμος* meaning tile).

*Experimental details.*—We conduct experiments on a two-dimensional granular system composed of  $N = 890$  bidisperse (Vishay PhotoStress PSM-4) circular disks with an equal fraction of radii  $R_s = 5.5$  mm and  $R_l = 7.7$  mm ( $R_l/R_s = 1.4$ ). A subfluidizing upflow of air passing through a porous polypropylene sheet floats the particles to eliminate basal friction. A rigid support grid ensures that the surface is level to reduce drift and smooth to prevent particle clustering. Further experimental details are provided in Ref. [8].

Each granular configuration is subject to quasistatic loading under one of three protocols: (i) uniaxial compression, (ii) biaxial compression, and (iii) simple shear, shown in Fig. 1. Under all protocols, the disks are initially confined to a square region of  $48 \times 48$  cm bounded by two walls controlled by stepper motors and two fixed walls. Under uniaxial compression, a single motorized wall compresses the system with a series of steps of constant size (0.6 mm), while under biaxial compression, both motorized walls compress the system with the same step size. The loading walls then retract, and the system dilates to a loose packing, activating a brief overheard flow of turbulent air which rearranges the particles to produce a new random configuration. Under simple shear, after slowly compressing to approach the jamming transition, one wall moves in while another moves out. We conduct the shear experiments under both combinations of the wall displacements (denoted by  $\text{shear}^A$  and  $\text{shear}^B$ ) to isolate the effects of experimental asymmetries such as boundary misalignment or height or gravity gradients.

We repeat the experiment to obtain at least 1000 packings under each protocol and, for each packing, capture images taken under polarized light which contain the photoelastic response to interparticle forces. We track particle positions using MATLAB and use `Voro++`, a Voronoï tessellation tool, to determine disk neighbors and local volumes [29]. From the polarized images, we determine the normal and tangential contact forces using nonlinear least-squares minimization between a numerically constructed fringe pattern and the actual image [30,31]. This provides the forces  $\vec{F}_{\mu\nu}$  and relative positions  $\vec{r}_{\mu\nu}$  needed to construct the force-moment tensor. The full data set is available for download in Ref. [32].

Local free volumes, preferred to global values for particle-scale statistical mechanics [33–36], are calculated for clusters of  $m = 8$  particles, using the  $m - 1$  particles nearest to each central particle. To account for the particle bidispersity [37], we determine the local free volume of a cluster from  $v^f = (1/m) \sum_i v_i - v_{\min}(R_i)$ , where  $R_i$  is  $R_s$  (or  $R_l$ ) for small (or large) particles and  $v_i$  is the corresponding particle Voronoï volume. Normalizing by the smallest possible Voronoï volume  $v_{\min}$  and averaging over many randomly selected clusters yields the global measure  $\tilde{v}^f = \langle v^f/v_{\min} \rangle$ . Figure 1(b) demonstrates that histograms of the mean local free volume  $\tilde{v}^f$  and global confining pressure  $\Gamma = (1/N)\text{Tr}(\hat{\Sigma})$  vary depending on the loading protocol. Note that this “pressure” has units of Nm instead of the usual 2D pressure N/m<sup>2</sup>, since we have chosen, for simplicity, not to divide by the particle area.

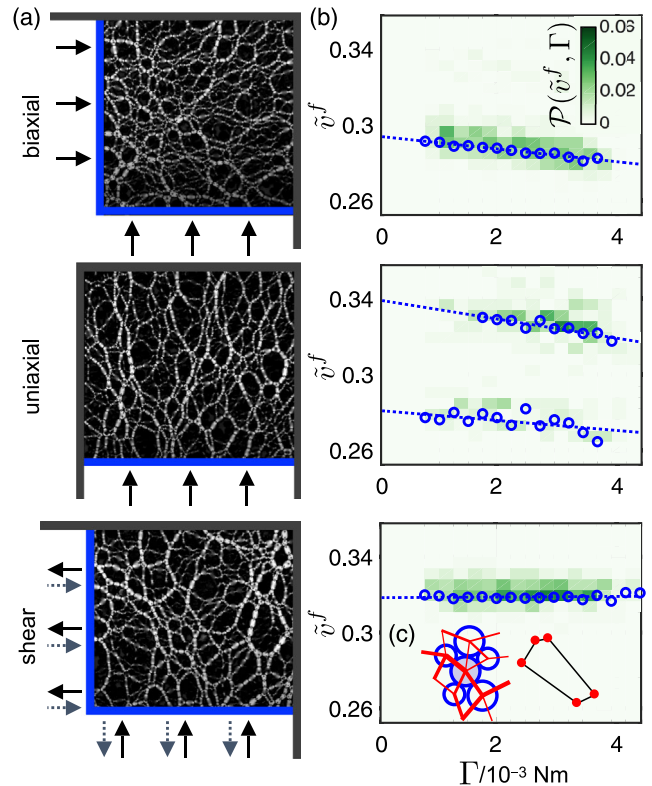


FIG. 1. (a) Example photoelastic images at  $\Gamma = 2.1 \times 10^{-3}$  Nm for each of three loading schemes—biaxial, uniaxial, and  $\text{shear}^A$ —shown schematically according to which walls move.  $\text{Shear}^B$  (dashed lines) is the opposite of  $\text{shear}^A$  (solid lines). Bright particles are under larger force; large-scale light gradients have been removed by image processing. (b) Joint probability distributions  $\mathcal{P}(\tilde{v}^f, \Gamma)$  for dimensionless mean local free volume  $\tilde{v}^f$  (averaged over clusters of size  $m = 8$ ) and global confining pressure  $\Gamma$  for each protocol. Dashed lines are linear fits using a weighted average. (c) A force-balanced particle within a jammed packing has an associated Maxwell-Cremona tile, formed by a closed loop of all vector forces acting on a particle.

We observe that across all three protocols there are two characteristic mean free volumes:  $\tilde{v}^f \approx 0.28$  observed for biaxial loading and  $\tilde{v}^f \approx 0.32$  observed for shear loading. The looser-packed value for sheared samples is expected from Reynolds dilatancy and the Poynting effect [38–41]. States prepared by uniaxial compression exhibit both values, in line with principal component analysis [42]. Along each  $\tilde{v}^f(\Gamma)$  characteristic curve, we observe that  $\tilde{v}^f$  decreases approximately linearly as a function of  $\Gamma$ , except in the case of shear, which by experimental design was constrained to constant volume and therefore free volume.

*Measuring temperaturelike quantities.*—In the absence of an explicitly known partition function, we measure the temperaturelike quantities  $(\hat{\alpha}, \kappa)$  using the method of overlapping histograms [43,44], as has previously been applied to granular ensembles [7,8,13,35]. We construct histograms of the components of  $\hat{\sigma}$  over the entire range of  $(\tilde{v}^f, \Gamma)$  shown in Fig. 1, binning states by the global measure  $\Gamma$ . We neglect data with  $\Gamma < 10^{-3}$  Nm, set by the lower limit of our force resolution. From within each packing, we randomly generate clusters of size  $m = 8$  from nearby disks. For each cluster, the force-moment tensor is computed additively over the particles in the cluster and can be resolved into a normal  $p = (\sigma_1 + \sigma_2)/2$  and deviatoric  $\tau = (\sigma_1 - \sigma_2)/2$  components for eigenvalues  $\sigma_1$  and  $\sigma_2$ . As observed by Refs. [7,8],  $m = 8$  is large enough that measurements of temperaturelike variables are independent of  $m$ .

Under each of the four protocols, we compute the two associated distributions of the force-moment tensor,  $\mathcal{P}(p|\Gamma)$  and  $\mathcal{P}(\tau|\Gamma)$ . As shown in Fig. 2 and 3, we observe that, as confining pressure increases, the distributions of both normal and deviatoric components broaden [7–9,13]. Note that the states prepared under the two different shear-loading protocols (A and B) were found to exhibit spontaneous symmetry breaking, resulting in a bias towards negative and positive deviatoric components, respectively [45]. Consequently, we treat these two protocols separately. For  $\mathcal{P}(p)$  in both shear protocols, the mean and variance are indistinguishable from each other, while for  $\mathcal{P}(\tau)$ , the mean is translated in opposite directions.

To proceed with the overlapping histogram methods, we utilize the ratio  $\mathcal{R}^\sigma(\sigma, \Gamma_i, \Gamma_j) \equiv \log[\mathcal{P}(\sigma|\Gamma_i)/\mathcal{P}(\sigma|\Gamma_j)]$  with  $\sigma$  being either  $p$  or  $\tau$ . To give this ratio more meaning, consider the distribution of Eq. (1) under the assumption that (i) the local force-tiling area  $a$  is strongly peaked at  $\det(\hat{\sigma})$  [10,11,13] and (ii) the off-diagonal components of the local stress  $\hat{\sigma}$  are small compared to the diagonal elements (see Supplemental Material [46]). For isotropically prepared states, the normal stress typically dominates the deviatoric stress [24,27]. In this limit, we can integrate Eq. (1) to isolate distributions:

$$\mathcal{P}(p|\Gamma) = \frac{\tilde{\Omega}(p, \Gamma)}{Z(\hat{\alpha}, \kappa)} \exp(-\alpha^p p - \kappa p^2), \quad (2)$$

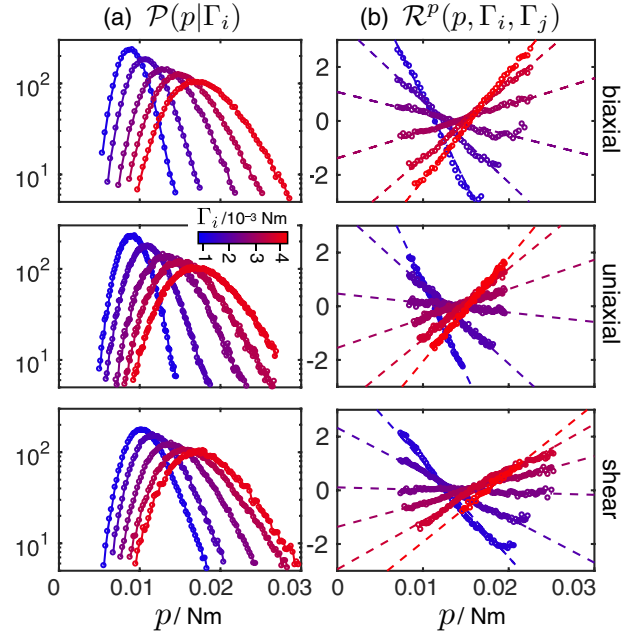


FIG. 2. (a) Histograms of local normal force-moment component  $p$  on clusters of  $m = 8$  particles, at fixed  $\Gamma_i$ , for all three loading protocols (shear<sup>A</sup> and shear<sup>B</sup> combined). (b) Associated histogram log-ratios  $\mathcal{R}$  taken between probability distributions observed at confining pressure  $\Gamma_i$  and  $\Gamma_j = \frac{1}{2} \max(\Gamma_i)$ . Each  $\mathcal{R}(p)$  is fit to a straight line with slope  $\alpha_j^p - \alpha_i^p$  [Eq. (4), with  $\kappa_j - \kappa_i \approx 0$ ].

$$\mathcal{P}(\tau|\Gamma) = \frac{\hat{\Omega}(\tau, \Gamma)}{Z(\hat{\alpha}, \kappa)} \exp(-\alpha^\tau \tau + \kappa \tau^2), \quad (3)$$

for modified densities of state  $\hat{\Omega}$  and  $\tilde{\Omega}$  (see Supplemental Material [46]). Thus, we have three temperaturelike quantities:  $\alpha^p$  and  $\alpha^\tau$ , the normal and deviatoric components of the angoricity tensor, and  $\kappa$ , the keramicity. By taking the logarithm ratios of these two distributions, Eqs. (2) and (3) are, respectively,

$$\mathcal{R}^p(p, \Gamma_i, \Gamma_j) = \mathcal{R}_0^p + (\alpha_j^p - \alpha_i^p)p + (\kappa_j - \kappa_i)p^2, \quad (4)$$

$$\mathcal{R}^\tau(\tau, \Gamma_i, \Gamma_j) = \mathcal{R}_0^\tau + (\alpha_j^\tau - \alpha_i^\tau)\tau - (\kappa_j - \kappa_i)\tau^2, \quad (5)$$

where  $\mathcal{R}_0 = \log(Z_i/Z_j)$  and  $(i, j)$  denotes two sets of states of pressure  $\Gamma_i$  and  $\Gamma_j$  (see Supplemental Material [46]). Because ratios are sensitive to counting errors in small values of the denominator, we examine only data for which  $\mathcal{P} > 10$ .

In Figs. 2(b) and 3(b), we illustrate typical logarithm ratios for several representative histograms; all ratios are computed relative to the same reference histogram. We observe that  $\mathcal{R}^p$  is linear in  $p$  with some arbitrary offset associated with the ratio of partition functions. The slope of  $\mathcal{R}^p(p)$  gives the differential normal angoricity,  $\alpha_j^p - \alpha_i^p$  between states at confining pressures  $\Gamma_j$  and  $\Gamma_i$ . However, the ratios in Fig. 2(b) do not provide confident fits beyond a

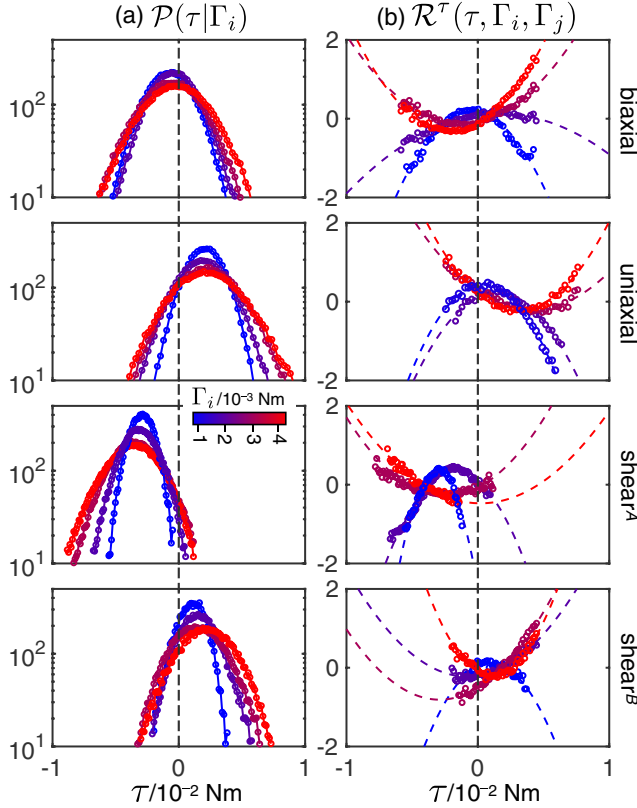


FIG. 3. (a) Histograms of local deviatoric force-moment component  $\tau$  on clusters of  $m = 8$  particles, at fixed  $\Gamma_i$ , for all four loading protocols (shear<sup>A</sup> and shear<sup>B</sup> separated). (b) Associated histogram log-ratios  $\mathcal{R}$  taken between probability distributions observed at confining pressure  $\Gamma_i$  and  $\Gamma_j = \frac{1}{2} \max(\Gamma_i)$ . Each  $\mathcal{R}(\tau)$  is fit to a parabola with coefficients  $\alpha_j^\tau - \alpha_i^\tau$  and  $\kappa_j - \kappa_i$  [Eq. (5)].

first-order polynomial in  $p$ , such that the difference  $\kappa_j - \kappa_i$  cannot be established from this approach due to experimental limitations in the range of  $p$  [13].

In contrast, similar ratios computed in Fig. 3(b) are found to be parabolic with a nonzero second-order coefficient,

matching the expectation from Eq. (5), and we fit these ratios to a polynomial:  $x\tau^2 + y\tau + z$ . The fit parameter  $x$ , corresponding to changes in the variance of force-moment component distributions, gives  $x = \kappa_i - \kappa_j$ , the difference in keramicity between states of global confining pressure  $\Gamma_i$  and  $\Gamma_j$ . As before, we also identify the fit parameter  $y$  to be associated with  $y = \alpha_j^\tau - \alpha_i^\tau$ . Thus, by taking the logarithm of the ratio of two closely overlapped histograms with sufficient proximity in local free volume [7], we can compute relative measures of  $\alpha^p$ ,  $\alpha^\tau$ , and  $\kappa$  to within an additive constant  $\mathcal{R}_0$  [8].

The presence of a  $\tau^2$  term is found for all three protocols, in agreement with predictions by Wu and Teitel [13], in which the multipliers  $\alpha^p$  and  $\kappa$  are strictly related to only global measures of pressure. This allows the Boltzmann-like factor found in Eq. (1) to include terms that are quadratic in the components of the force-moment tensor.

*Equations of state.*—As shown for angoricity under isotropic compression, we propose that the computed temperaturelike state variables can be described by equations of state of the form  $\alpha\Gamma = \lambda$  [7,8,47], where  $\alpha$  represents any of  $(\alpha^p, \alpha^\tau, \kappa)$  and  $\lambda$  is a constant. To test experimental adherence to this hypothesis, we identify  $(1/\alpha) = 0$  (and  $(1/\kappa) = 0$ ) as corresponding to the jamming point ( $\Gamma = 0$ ) and reference temperaturelike variable measurements accordingly (see Supplemental Material [46]).

Repeating this procedure for all three temperaturelike variables, we observe that the equation of state holds in all cases (Fig. 4). While for  $\kappa$  the constant  $\lambda$  is independent of loading protocol, for both  $\alpha^p$  and  $\alpha^\tau$  the constant exhibits significant protocol dependence. Interestingly,  $\lambda$  is always positive for  $\alpha^p$ , but the sign varies for  $\alpha^\tau$  (values given in the caption), corresponding to the direction of translation of  $\mathcal{P}(\tau)$  in Fig. 3(a), some of which are associated with experimental asymmetries. The magnitudes of the  $\lambda$  agree within 2 standard errors for shear<sup>A</sup> vs shear<sup>B</sup>, and the signs

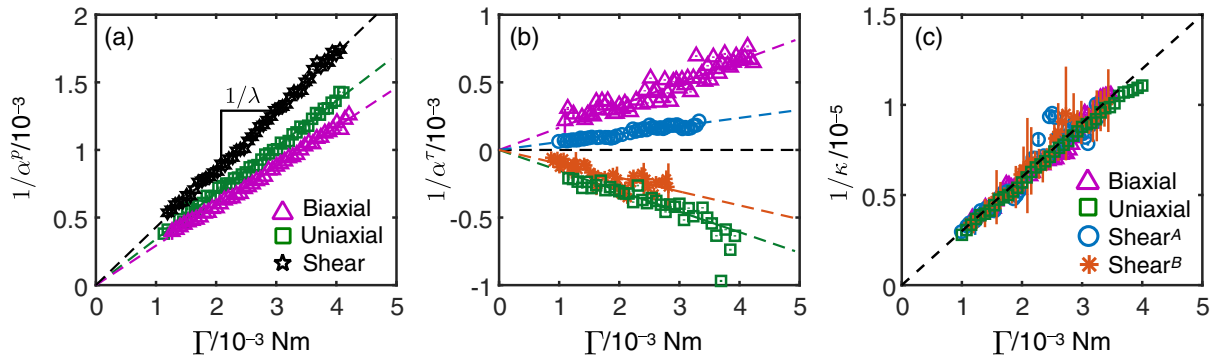


FIG. 4. Temperaturelike variables: (a) Normal inverse angoricity,  $1/\alpha^p$  against confining pressure  $\Gamma$ , as computed for three loading conditions [ $(\alpha^p\Gamma)^{-1} = 0.29 \pm 0.01$  (biaxial),  $0.34 \pm 0.01$  (uniaxial), and  $0.43 \pm 0.01$  (shear)]. (b) Deviatoric inverse angoricity,  $1/\alpha^\tau$  plotted against the same, indicating opposite dependencies on confining pressure based on the loading protocol [ $(\alpha^\tau\Gamma)^{-1} = -1.5 \pm 0.1$  (uniaxial),  $1.6 \pm 0.1$  (biaxial),  $0.59 \pm 0.03$  (shear<sup>A</sup>), and  $-1.0 \pm 0.3$  (shear<sup>B</sup>)]. (c) The inverse keramicity ( $1/\kappa$ ) evolves linearly with confining pressure and does so with equal proportionality under all protocols [ $(\kappa\Gamma)^{-1} = (3.0 \pm 0.1) \times 10^{-3}$ ]. Dashed lines represent linear fits.

differ due to the change in sign of  $\tau$ . Because both components of  $\hat{\alpha}$  are observed to be protocol dependent, the tensorial angoricity is not valid as a variable of *state* but rather a variable of *process*. By contrast, the keramicity behaves as a state variable.

Angoricity measures a granular packing's ability to accommodate configurational rearrangements of the equivalent global force-moment tensor (equivalently, stress) on a componentwise basis,  $\alpha_{ij} = \partial S / \partial \Sigma_{ij}$ . Thus, we have shown that, as packings are loaded above jamming, they gain more configurations from the presence of forces to be distributed [Fig. 4(a)]. Meanwhile, as  $(1/\alpha^p)$  [Fig. 4(a)] and  $(1/\alpha^\tau)$  [Fig. 4(b)] grow in magnitude, the responsiveness of the number of configurations to increases in global stress ( $\partial S / \partial \Sigma$ , where  $\Sigma$  is either the normal or deviatoric component of  $\hat{\Sigma}$ ) decreases. Finally, the protocol by which a granular packing is loaded does not impact the trend that more compressed states gain fewer additional configurations from equivalent additions to the global Maxwell-Cremona area tiling [Fig. 4(c)].

*Conclusion.*—We have demonstrated non-negligible curvature in the ratio of overlapped force-moment tensor histograms in jammed states of granular systems. This observation points towards a formulation of the force-moment ensemble that requires the conservation of Maxwell-Cremona area tiling. The associated temperature-like variables all grow inversely with respect to confining pressure, but the keramicity, associated with the force tiling, is the only valid variable of state. The path dependence of variables describing soft matter systems is not unfamiliar, but protocol-dependent scaling could be a route to a comprehensive granular equation of state. Meanwhile, the generalization of the force-moment ensemble to account for force-tiling statistics may yield a comprehensive statistical mechanics framework.

We are grateful for support from the National Science Foundation (DMR-1206808) and James S. McDonnell Foundation and for useful conversations with Bob Behringer, Rafi Blumenfeld, Bulbul Chakraborty, Daphne Klotsa, James Puckett, Steve Teitel, and Brian Tighe.

---

[1] S. F. Edwards and R. B. S. Oakeshott, *Physica A* **157**, 1080 (1989).  
 [2] H. M. Jaeger and S. R. Nagel, *Science* **255**, 1523 (1992).  
 [3] R. C. Ball and R. Blumenfeld, *Phys. Rev. Lett.* **88**, 115505 (2002).  
 [4] S. Martiniani, K. J. Schrenk, K. Ramola, B. Chakraborty, and D. Frenkel, *Nat. Phys.*, **13**, 848 (2017).  
 [5] K. Ramola and B. Chakraborty, *J. Stat. Phys.* **169**, 1 (2017).  
 [6] D. Bi, S. Henkes, K. E. Daniels, and B. Chakraborty, *Annu. Rev. Condens. Matter Phys.* **6**, 63 (2015).  
 [7] S. Henkes, C. S. O'Hern, and B. Chakraborty, *Phys. Rev. Lett.* **99**, 038002 (2007).  
 [8] J. G. Puckett and K. E. Daniels, *Phys. Rev. Lett.* **110**, 058001 (2013).

[9] R. Blumenfeld and S. F. Edwards, *J. Phys. Chem. B* **113**, 3981 (2009).  
 [10] B. P. Tighe, A. R. T. van Eerd, and T. J. H. Vlugt, *Phys. Rev. Lett.* **100**, 238001 (2008).  
 [11] B. P. Tighe and T. J. H. Vlugt, *J. Stat. Mech.* (2011) P04002.  
 [12] I. Jorjadze, L.-L. Pontani, and J. Brujic, *Phys. Rev. Lett.* **110**, 048302 (2013).  
 [13] Y. Wu and S. Teitel, *Phys. Rev. E* **92**, 022207 (2015).  
 [14] S. Sarkar, D. Bi, J. Zhang, J. Ren, R. P. Behringer, and B. Chakraborty, *Phys. Rev. E* **93**, 042901 (2016).  
 [15] E. DeGiuli, *Phys. Rev. Lett.* **121**, 118001 (2018).  
 [16] E. DeGiuli, *Phys. Rev. E* **98**, 033001 (2018).  
 [17] T. S. Majmudar and R. P. Behringer, *Nature (London)* **435**, 1079 (2005).  
 [18] T. Bertrand, R. P. Behringer, B. Chakraborty, C. S. O'Hern, and M. D. Shattuck, *Phys. Rev. E* **93**, 012901 (2016).  
 [19] P. Chaudhuri, L. Berthier, and S. Sastry, *Phys. Rev. Lett.* **104**, 165701 (2010).  
 [20] J. D. Paulsen, N. C. Keim, and S. R. Nagel, *Phys. Rev. Lett.* **113**, 068301 (2014).  
 [21] C. Josserand, A. V. Tkachenko, D. M. Mueth, and H. M. Jaeger, *Phys. Rev. Lett.* **85**, 3632 (2000).  
 [22] S. M. Rubinstein, G. Cohen, and J. Fineberg, *Phys. Rev. Lett.* **96**, 256103 (2006).  
 [23] M. Huang and J. P. Sethna, *Phys. Rev. B* **43**, 3245 (1991).  
 [24] D. Bi, J. Zhang, B. Chakraborty, and R. P. Behringer, *Nature (London)* **480**, 355 (2011).  
 [25] H. A. Vinutha and S. Sastry, *Nat. Phys.* **12**, 578 (2016).  
 [26] A. J. Liu and S. R. Nagel, *Annu. Rev. Condens. Matter Phys.* **1**, 347 (2010).  
 [27] D. Bi, J. Zhang, R. P. Behringer, and B. Chakraborty, *Europhys. Lett.* **102**, 34002 (2013).  
 [28] B. Chakraborty, *Soft Matter* **6**, 2884 (2010).  
 [29] C. H. Rycroft, G. S. Grest, J. W. Landry, and M. Z. Bazant, *Phys. Rev. E* **74**, 021306 (2006).  
 [30] K. E. Daniels, J. E. Kollmer, and J. G. Puckett, *Rev. Sci. Instrum.* **88**, 051808 (2017).  
 [31] J. E. Kollmer, Photo-Elastic Grain Solver, <http://github.com/jekollmer/PEGS>.  
 [32] DOI: 10.5061/dryad.9jp26bk  
 [33] C. Song, P. Wang, and H. A. Makse, *Nature (London)* **453**, 629 (2008).  
 [34] T. Aste and T. Di Matteo, *Phys. Rev. E* **77**, 021309 (2008).  
 [35] S. McNamara, P. Richard, S. K. de Richter, G. Le Caër, and R. Delannay, *Phys. Rev. E* **80**, 031301 (2009).  
 [36] I. Jorjadze, L. L. Pontani, and J. Brujic, *Phys. Rev. Lett.* **110**, 048302 (2013).  
 [37] F. Lechenault, F. da Cruz, O. Dauchot, and E. Bertin, *J. Stat. Mech.* (2006) P07009.  
 [38] J. Ren, J. A. Dijksman, and R. P. Behringer, *Phys. Rev. Lett.* **110**, 018302 (2013).  
 [39] B. Andreotti, Y. Forterre, and O. Pouliquen, *Granular Media: Between Fluid and Solid* (Cambridge University Press, Cambridge, England, 2013).  
 [40] B. P. Tighe, *Granular Matter* **16**, 203 (2014).  
 [41] K. Baumgarten and B. P. Tighe, *Phys. Rev. Lett.* **120**, 148004 (2018).  
 [42] H. Hotelling, *Analysis of a Complex of Statistical Variables into Principal Components* (Warwick & York, Baltimore, MD, 1933).

- [43] P. Labastie and R. L. Whetten, *Phys. Rev. Lett.* **65**, 1567 (1990).
- [44] D. S. Dean and A. Lefèvre, *Phys. Rev. Lett.* **90**, 198301 (2003).
- [45] T. B. Nguyen and A. Amon, *Europhys. Lett.* **116**, 28007 (2016).
- [46] See Supplemental Material at <http://link.aps.org/supplemental/10.1103/PhysRevLett.122.038001> for details on the overlapping histogram method and the determination of anisotropy.
- [47] S. Henkes and B. Chakraborty, *Phys. Rev. Lett.* **95**, 198002 (2005).